# Thermo-optic characterization of Yb:CaGdAlO4 laser crystal

**Article** *in* Optical Materials Express · November 2014

Impact Factor: 2.84 · DOI: 10.1364/OME.4.002241

# Thermo-optic characterization of Yb:$CaGdAlO_4$ laser crystal

**Pavel Loiko,[1] Frederic Druon,[2,*] Patrick Georges,[2] Bruno Viana,[3] and Konstantin Yumashev[1]**

[1]*Center for Optical Materials and Technologies, Belarusian National Technical University, 220013 Minsk, Belarus*
[2]*Laboratoire Charles Fabry, Institut d'Optique, CNRS, Univ Paris Sud, Palaiseau, France*
[3]*IRCP, Institut de Recherche de Chimie Paris, CNRS Chimie Paristech, 11 rue P et M Curie, 75005 Paris, France*
[*]*frederic.druon@institutoptique.fr*

**Abstract:** Principal thermo-optic coefficients (TOCs), $dn_o/dT$ and $dn_e/dT$, are measured for Yb:$CaGdAlO_4$ crystal, for the first time, to our knowledge. At the wavelength of ~1 μm, they equal –7.6 and –8.6 ($\times 10^{-6}$ $K^{-1}$), accordingly. Thermal coefficients of the optical path (TCOP) are determined for this crystal for the principal crystal cuts (***a***-cut and ***c***-cut) and light polarizations ($\pi$ or $\sigma$). Thermo-optic dispersion formulas are evaluated for both TOC and TCOP coefficients. Optical power of thermal lens is measured for diode-pumped ***a***-cut Yb:$CaGdAlO_4$; it is also calculated on the basis of measured material parameters. Thermal conductivity of $CaGdAlO_4$ crystal is measured versus Yb concentration. The results indicate that ***a***-cut Yb:$CaGdAlO_4$ can provide really "athermal" behavior.



**OCIS codes:** (140.3380) Laser materials; (140.6810) Thermal effects; (140.3480) Lasers, diode-pumped.

## References and links

1. S. Chénais, F. Druon, S. Forget, F. Balembois, and P. Georges, "On thermal effects in solid-state lasers: the case of ytterbium-doped materials," Progr. Quantum Electron. **30,** 89-153 (2006).
2. J. Petit, P. Goldner, and B. Viana, "Laser emission with low quantum defect in Yb:$CaGdAlO_4$," Opt. Lett. **30**, 1345–1347 (2005).
3. F. Druon, F. Balembois, and P. Georges "New Materials for Short-Pulse Amplifiers," IEEE Photonics Journal **3**, 268-273 (2011)
4. J. Boudeile, F. Druon, M. Hanna, P. Georges, Y. Zaouter, E. Cormier, J. Petit, P. Goldner, and B. Viana, "Continuous-wave and femtosecond laser operation of Yb:$CaGdAlO_4$ under high-power diode pumping," Opt. Lett. **32**, 1962-1964 (2007).
5. A. Guandalini, A. Greborio, and J. Aus der Au, "Sub-100-fs pulses with 12.5 W from Yb:CALGO based oscillators," presented at Solid State Lasers XXI: Technology and Devices (2012), paper 8235-31.
6. S. Ricaud, A. Jaffres, P. Loiseau, B. Viana, B. Weichelt, M. Abdou-Ahmed, A. Voss, T. Graf, D. Rytz, M. Delaigue, E. Mottay, P. Georges, and F. Druon, "Yb:$CaGdAlO_4$ thin-disk laser," Opt. Lett. **36**, 4134-4136 (2011).
7. K. Beil, B. Deppe, and C. Kränkel, "Yb:$CaGdAlO_4$ thin-disk laser with 70% slope efficiency and 90 nm wavelength tuning range," Opt. Lett. **38**, 1966-1968 (2013).
8. Y. Zaouter, J. Didierjean, F. Balembois, G. Lucas Leclin, F. Druon, P. Georges, J. Petit, P. Goldner and B. Viana "47-fs diode-pumped $Yb^{3+}$:$CaGdAlO_4$ laser," Opt. Lett. **31**, 119-121 (2006).
9. A. Agnesi, A. Greborio, F. Pirzio, G. Reali, J. A. der Au, and A. Guandalini, "40-fs $Yb^{3+}$:$CaGdAlO_4$ laser pumped by a single-mode 350-mW laser diode," Opt. Expr. **20**, 10077–10082 (2012).
10. P. Sevillano, P. Georges, F. Druon, D. Descamps, E. Cormier, "32-fs Kerr-lens mode-locked Yb:CALGO oscillator optically pumped by a bright fiber laser" Opt. Lett. **39**, (2014).
11. S. Ricaud, A. Jaffres, K. Wentsch, A. Suganuma, B. Viana, P. Loiseau, B. Weichelt, M. Abdou-Ahmed, A. Voss, T. Graf, D. Rytz, C. Hönninger, E. Mottay, P. Georges, and F. Druon, "Femtosecond Yb:$CaGdAlO_4$ thin-disk oscillator," Opt. Lett. **37**, 3984-3986 (2012).
12. A. Diebold, F. Emaury, C. Schriber, M. Golling, C. J. Saraceno, T. Südmeyer, and U. Keller, "SESAM mode-locked Yb:$CaGdAlO_4$ thin disk laser with 62 fs pulse generation," Opt. Lett. **38**, 3842–3845 (2013).
13. E. Caracciolo, M. Kemnitzer, A. Guandalini, F. Pirzio, J. Aus der Au, and A. Agnesi, "28-W, 217 fs solid-state Yb:$CAlGdO_4$ regenerative amplifiers," Opt. Lett. **38**, 4131-4133 (2013).

14. J. Pouysegur, M. Delaigue, Y. Zaouter, C. Hönninger, E. Mottay, A. Jaffrès, P. Loiseau, B. Viana, P. Georges, and F. Druon, "Sub-100-fs Yb:CALGO nonlinear regenerative amplifier," Opt. Lett. **38**, 5180-5183 (2013).
15. F. Druon, M. Olivier, A. Jaffrès, P. Loiseau, N. Aubry, J. DidierJean, F. Balembois, B. Viana, and P. Georges, "Magic mode switching in Yb:$CaGdAlO_4$ laser under high pump power," Opt. Lett. **38**, 4138-4141 (2013).
16. S.P. Timoshenko, J. N. Goodier, Theory of Elasticity, 3nd ed. (McGraw-Hill, New York, 1987), Chap. 13.
17. S. Vatnik, M.C. Pujol, J.J. Carvajal, X. Mateos, M. Aguiló, F. Díaz, and V. Petrov, "Thermo-optic coefficients of monoclinic $KLu(WO_4)_2$," Appl. Phys. B **95**, 653–556 (2009).
18. S. Biswal, S.P. O'Connor, and S.R. Bowman, "Thermo-optical parameters measured in ytterbium-doped potassium gadolinium tungstate," Appl. Opt. **44**, 3093–3097 (2005).
19. P.A. Loiko, V.V. Filippov, K.V. Yumashev, N.V. Kuleshov, and A.A. Pavlyuk, "Thermo-optic coefficients study in $KGd(WO_4)_2$ and $KY(WO_4)_2$ by a modified minimum deviation method," Appl. Opt. **51**, 2951–2957 (2012).
20. P.A. Loiko, K.V. Yumashev, N.V. Kuleshov, and A.A. Pavlyuk, "Thermooptic coefficients of Nd-doped anisotropic $KGd(WO_4)_2$, $YVO_4$ and $GdVO_4$ laser crystals," Appl. Phys. B **102**, 117–122 (2011).
21. P. Loiko, K. Yumashev, N. Kuleshov, G. Rachkovskaya, and A. Pavlyuk, "Thermo-optic dispersion formulas for monoclinic double tungstates $KRe(WO_4)_2$ where Re = Gd, Y, Lu, Yb," Opt. Mater. **33**, 1688–1694 (2011).
22. J. Petit, "Monocristaux dopés ytterbium et matériaux assemblés pour lasers de fortes puissances", PhD Chimie Paritech, 2006.
23. A.A. Kaminskii, X. Xu, O. Lux, H. Rhee, H.J. Eichler, J. Zhang, D. Zhou, A. Shirakawa, K. Ueda, and J. Xu, "High-order stimulated Raman scattering in tetragonal $CaYAlO_4$ crystal-host for $Ln^{3+}$-lasant ions," Laser Phys. Lett. **9**, 306–311 (2012).
24. D. Li, X. Xu, H. Zhu, X. Chen, W.D. Tan, J. Zhang, D. Tang, J. Ma, F. Wu, C. Xia, and J. Xu, "Characterization of laser crystal Yb:$CaYAlO_4$," J. Opt. Soc. Am. B **28**, 1650–1654 (2011).
25. P. Loiko, K. Yumashev, V. Matrosov, and N. Kuleshov, "Dispersion and anisotropy of thermo-optic coefficients in tetragonal $GdVO_4$ and $YVO_4$ laser host crystals," Appl. Opt. **52**, 698–705 (2013).
26. P. Loiko, V. Kisel, N. Kondratuk, K. Yumashev, N. Kuleshov, and A. Pavlyuk, "14W high-efficiency diode-pumped cw Yb:$KGd(WO_4)_2$ laser with low thermo-optic aberrations," Opt. Mater. **35**, 582–585 (2013).
27. R. Gaumé, B. Viana, D. Vivien, J.-P. Roger, and D. Fournier, "A simple model for the prediction of thermal conductivity in pure and doped in insulating crystals," Appl. Phys. Lett. **83**, 1355–1357 (2003).

## 1. Introduction

Thermal lensing is one of the most important limitations for power scaling capabilities of diode-pumped solid-state lasers. With a lens-like crystal being placed in the laser cavity, one can observe abrupt drop of output power, distortions in the spatial profile of output beam, as well as depolarization losses [1]. Thus, detailed information about properties of thermal lens, as well as material parameters useful for their calculation, is crucial for laser design. In practice, this means knowledge of temperature variation of refractive index (expressed by $dn/dT$ coefficient), as well as optical path length (expressed by thermal coefficient of the optical path, TCOP).

In the present paper, we aim to perform experimental study of these parameters for Yb:$CaGdAlO_4$ (Yb:CALGO) laser crystal, for the first time, to our knowledge. The interest to Yb:CALGO is motivated by its beneficial spectroscopic and thermal properties [2,3], that allowed for realization of high-efficient and high-power bulk [4,5] and thin-disk lasers [6,7], as well as generation and amplification of ultrashort pulses [8-14] with pulse production as short as 32 fs [10]. However, Yb:CALGO demonstrate very particular thermal properties involving a strong anisotropy of its lattice. This anisotropy also implicates a strong anisotropy of the thermal properties of Yb:CALGO. This represents one of the key issues in the development of high power DPSSL using Yb:CALGO. Indeed, it has been observed that pumping above 100 W may involves strong thermal beam deformation, both in thin-disk or bulk configuration. On the first hand, in thin disk configuration [11], a thermal astigmatism has been identified as a limitation for high power production. On the second hand, in bulk configuration this time, it was recently demonstrated that Yb:CALGO can provide unique stabilization of laser mode at high pump powers [15], the effect that cannot be completely understood on the basis of reported properties up to now. This special behavior of Yb:CALGO clearly motivates a better and more accurate understanding of the thermal properties of this atypical crystal.

## 2. Laser beam deviation method

The method for determination of thermo-optic coefficients, d$n$/d$T$ or TOCs, is based on the measurement of deflection of a probe beam passed through the studied sample with a linear thermal gradient, see Fig. 1(a). The output beam of the probe laser is expanded and collimated with a pair of spherical lenses ($f$ = 20 and 100 mm); then its central part is cut with an iris (aperture of ~1 mm) small enough to provide near top-hat beam profile with a flat wavefront. The polarization of the probe beam is controlled with a Glan-Taylor polarizer. The latter can be varied for anisotropic crystals like Yb:CALGO, $\boldsymbol{E}_1$ and $\boldsymbol{E}_2$, as denoted in the figure. The sample has a rectangular shape with two opposite faces being in a thermal contact with Cu holders (by means of heat grease). The temperatures of "hot" and "cold" surfaces $T_h$ and $T_c$ are controlled with Peltier elements with the precision of ~0.1 °C; their values are ~50 °C and ~0 °C, respectively. This results in a linear thermal gradient in the studied sample; this gradient is oriented perpendicularly to the beam propagation direction. For the sample with 5 mm height $H$, this gradient $\Delta T/H$ is ~10 °C/mm.

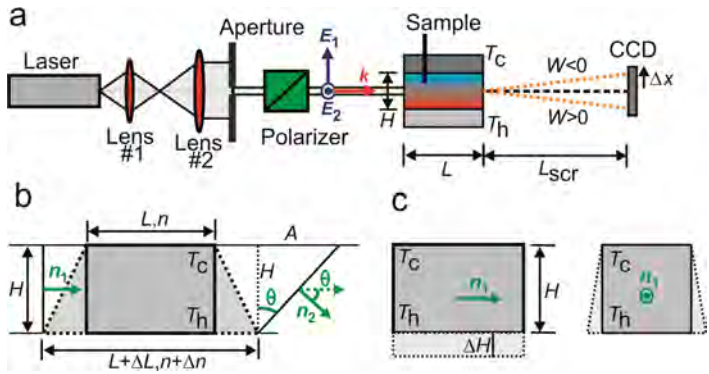


Fig. 1. Set-up representing laser beam deviation method for the measurement of thermo-optic coefficients (a), drawings for the calculation of the deviation angle $\theta$ (b,c), see explanations in the text.

Under these conditions, the probe beam deviates from the straightforward direction of its propagation (that is detected for the reference for uniform heating). The reason for this is elongation of the sample due to the thermal expansion, $\Delta L = \alpha L \Delta T$, where $L$ is the sample initial length; and variation of its refractive index $n$, expressed as $\Delta n$ = d$n$/d$T\Delta T$. Thus, the rays that propagate along the "hot" and "cold" surfaces of the crystal spend different time to travel $L+\Delta L$ distance, namely:

$$t_1 = (L+\Delta L)(n+\Delta n)/c, \quad (1a)$$

$$t_2 = Ln/c+\Delta L/c, \quad (1b)$$

respectively. Thus, the second ray is ahead on the distance $A = (t_1-t_2)/c$. This distance changes linearly when the first considered beam is shifter from the "hot" to the "cold" surface due to the linearity of the temperature distribution. Thus, a flat wavefront with a wave normal $\boldsymbol{n}_1$ is transferred to a flat one with a wave normal $\boldsymbol{n}_2$ rotated on a $\theta$ angle. This deviation angle can be calculated as $\tan\theta = A/H$. The same angle can be measured experimentally, considering the shift $\Delta x$ of the probe beam on a screen (we used a CCD-camera), as $\tan\theta = \Delta x/L_{scr}$ where $L_{scr}$ is the distance to the screen. The latter is chosen to be as long as 6 m to ensure good precision in the determination of small deviations (~ 5 μrad). The combination of these relations yields:

$$W = dn/dT + (n-1)\alpha = \frac{\Delta x}{L_{scr}} \frac{H}{L\cdot(T_h - T_c)}, \quad (2)$$

where the value $W$ is called thermal coefficient of the optical path (TCOP). The considered case results in the beam deviation to "cold" face (below, as shown in Fig. 1(a)), or $W > 0$. If one consider the case of $W < 0$ (that can be achieved for materials with negative d$n$/d$T$), the deviation is opposite. Thus, this method allows for the determination of $W$ sign. Calculation of

TOC then require the knowledge of refractive index for chosen light polarization and thermal expansion coefficient along the beam propagation direction. The precision of $W$ determination is ~$0.2\times10^{-6}$ $K^{-1}$. It should be noted that for a sample with a linear thermal gradient that is not fixed, thermal expansion effect does not produces thermal stresses that can lead to the variation of the optical path length [16]. The expansion of the sample along the thermal gradient, $\Delta H$, just produces a small variation of the deviation angle, $\Delta\theta < \theta$ that is below the measurement accuracy. The expansion in the third direction does not affect the experiment, see Fig. 1(c).

The laser beam deviation method was proposed by Vatnik to simplify the measurements of TOCs for anisotropic crystals, namely biaxial double tungstates [17]. To prove the correctness of the experiment, he used several crystal cuts providing access to the same light polarization (and, hence, the same $dn/dT$). Independent utilization of a high-precision interferometer-based approach [18], as well as minimum deviation method [19], shows rather good agreement (< $1\times10^{-6}$ $K^{-1}$) of all reported data. The case of uniaxial crystals is considered in [20].

### 3. Thermo-optic coefficients

Yb:CALGO is uniaxial, its optical axis is parallel to the ***c*** crystallographic one [2]. Thus, two principal TOCs exist, namely $dn_o/dT$ and $dn_e/dT$ (for ordinary and extraordinary rays). In order to determine them, we use the above mentioned laser beam deviation method. For this, one parallelepiped sample of 5at.%Yb:CALGO with the dimensions of $8(\boldsymbol{a})\times5(\boldsymbol{c})\times3.24$ $mm^3$ was used. Laser emission was propagating along the shorter edge, so two light polarizations, $\boldsymbol{E}\perp\boldsymbol{c}$ (*o*-wave) and $\boldsymbol{E}\parallel\boldsymbol{c}$ (*e*-wave), were available. The measurements were performed at 400, 532, 633, 652, 780, 810 and 1064 nm.

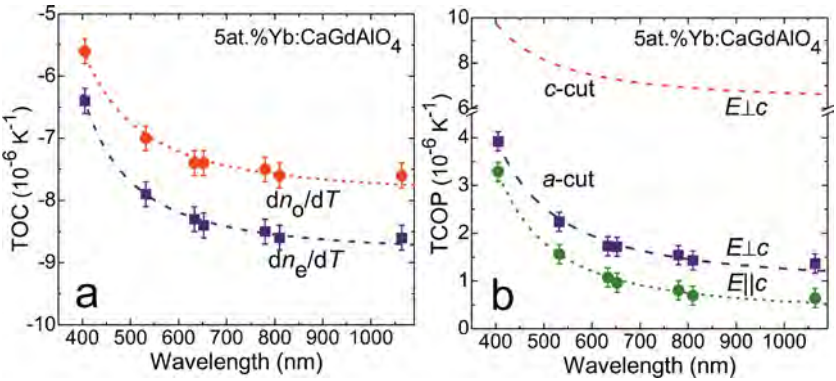


Fig. 2. Dispersion of thermo-optic coefficients (TOCs), $dn_o/dT$ and $dn_e/dT$, (a) and thermal coefficients of the optical path (TCOP), $W = dn/dT+(n-1)\alpha$, (b) for $Yb:CaGdAlO_4$ crystal: *points* are the experimental data, *curves* are their fitting.

**Table 1. Expansion Coefficients in the Thermo-Optic Dispersion Formulas for 5at%Yb:CaGdAlO$_4$ Laser Crystal**

| TOC/TCOP | Expansion coefficient | | | |
|---|---|---|---|---|
| | $A_0$ | $A_1$ | $A_2$ | $A_3$ |
| $dn_o/dT$ | -7.93 | 0.20 | 0.016 | 0.0021 |
| $dn_e/dT$ | -8.87 | 0.17 | 0.017 | 0.0035 |
| $W(\boldsymbol{a}\text{-cut}, \sigma)$ | 0.94 | 0.30 | 0.017 | 0.0021 |
| $W(\boldsymbol{a}\text{-cut}, \pi)$ | 0.31 | 0.25 | 0.017 | 0.0035 |

The results are presented in Fig. 2(a) as points. Both $dn/dT$ values are negative and satisfy the relation $dn_o/dT > dn_e/dT$. The dispersion of TOCs was modeled, taking into account temperature-dependence of bandgap, as well as volumetric thermal expansion [21], see curves in Fig. 1(a). This allows for evaluation of analytic expressions for the thermo-optic dispersion formulas:

$$\frac{dn}{dT}(\lambda) = A_0 + \frac{A_1}{\lambda^2} + \frac{A_2}{\lambda^4} + \frac{A_3}{\lambda^6}. \quad (3)$$

Here $dn/dT$ is expressed in $10^{-6}$ K$^{-1}$, light wavelength $\lambda$ – in μm, $A_{0\text{-}3}$ are the expansion coefficients. Their values are listed in Table 1. Thus, we were able to calculate both principal TOCs precisely at 1.03 μm, $dn_o/dT = -7.6$ and $dn_e/dT = -8.6\times10^{-6}$ K$^{-1}$.

Thermal expansion coefficients $\alpha$ of Yb:CALGO were measured with the same sample by means of a horizontal dilatometer Netzsch 402 PC in the temperature range of RT–200 °C (RT is the room temperature). Their value for the directions of ***a*** and ***c*** crystallographic axes are $\alpha_a$ = 10.0 and $\alpha_c$=16.2×10$^{-6}$ K$^{-1}$. The anisotropy of thermal expansion effect for $CaGdAlO_4$ and isostructural $CaYAlO_4$ crystals is analyzed in Table 2.

**Table 2. Thermal Expansion Coefficients Along *a* and *c* Axes [$10^{-6}$ K$^{-1}$] for Ca*R*AlO$_4$ Crystals**

| Crystal | $\alpha_a$ | $\alpha_c$ | $\alpha_a/\alpha_c$ | $\alpha_{vol}$ | Ref. |
|---|---|---|---|---|---|
| Ca*Gd*AlO$_4$ | 10.0 | 16.0 | 1.6 | 36.0 | This paper |
| | 10.1 | 16.2 | 1.6 | 36.4 | [22] |
| Ca*Y*AlO$_4$ | 8.0 | 11.0 | 1.4 | 27.0 | [23] |
| | 9.9 | 10.0 | 1.0 | 9.8 | [24] |

Thermal coefficient of the optical path for a laser crystal placed in the laser cavity, $W$, equals $dn/dT+(n-1)\alpha$. Here $n$ is the refractive index, and $\alpha$ is the thermal expansion coefficient in the direction of light propagation. For an ***a***-cut uniaxial crystal, there are two principal TCOP values, namely $W_1 = dn_e/dT + (n_e-1)\alpha_a$ for light polarization $\boldsymbol{E} \parallel \boldsymbol{c}$ ($\pi$), and $W_2 = dn_o/dT + (n_o-1)\alpha_a$ for $\boldsymbol{E} \perp \boldsymbol{c}$ ($\sigma$). Both these values were determined for ***a***-cut Yb:CALGO crystal with a laser beam deviation method, see points in Fig. 2(b).

The dispersion of TCOP coefficients was modeled in the manner similar to $dn/dT$ ones (see curves in Fig. 2(b), the corresponding expansion coefficients are listed in Table 1). In addition, TCOP was re-calculated for a ***c***-cut crystal. In this case, $W_3 = dn_o/dT + (n_o-1)\alpha_c$ for any light polarization. All three TCOP values are positive and possess a strong anisotropy. Indeed, at the wavelength of 1.03 μm and for ***a***-cut Yb:CALGO, $W$ = +1.3 $10^{-6}$K$^{-1}$ for $\sigma$-polarized light and only +0.7 for $\pi$-polarized, while it is near 6 times higher for ***c***-cut crystal: $W$ = +6.6 [$10^{-6}$ K$^{-1}$]. From this point of view, ***c***-cut Yb:CALGO crystal is the less suitable for power scaling due to strong detrimental thermal effects (compared with ***a***-cut). On the other hand, the ***c***-cut has the advantage to be isotropic in polarization and symmetric for the thermal lens shape. The summary of thermo-optic properties of Yb:CALGO is presented in Table 3.

**Table 3. Principal TOC and TCOP [$10^{-6}$ K$^{-1}$] for Yb:CaGdAlO$_4$ Laser Crystal at 1.03 μm**

| | $dn/dT$ | $dn/dT+(n\text{-}1)\alpha$ | | $\chi$* [15] |
|---|---|---|---|---|
| | | ***a***-cut | ***c***-cut | ***a***-cut |
| $\boldsymbol{E} \parallel \boldsymbol{a}$ | –7.6 | +1.3 | +6.6 | +1.3 (\|\| ***a***) |
| | | | | +1.3 (\|\| ***c***) |
| $\boldsymbol{E} \parallel \boldsymbol{c}$ | –8.6 | +0.7 | – | +0.6 (\|\| ***a***) |
| | | | | +0.9 (\|\| ***c***) |

*The values of "generalized" thermo-optic coefficient.

Yb:CALGO cut along the ***a*** axis provide near-zero and positive variation of the optical path length, OPL, (for $\pi$-polarization), the behavior that is called "athermal" [18]. Particularly for Yb:CALGO, it is related with (i) large and negative $dn/dT$ coefficients and (ii) large and strongly anisotropic thermal expansion.

## 4. Thermal lensing

Optical power of thermal lens $D$ (diopter, inverse of the focal length $f$), depends linearly on the absorbed pump power [1]. This dependence is typically expressed by the slope

(sensitivity factor of the thermal lens), $M = dD/dP_{abs}$ [25]. The $M$-factor vs. pump spot radius dependence for an ***a***-cut Yb:CALGO is presented in Fig. 3(a) (the details of such calculation can be found elsewhere [25]). Lasing at $\sigma$-polarization will produce stronger thermal lens (as compared with $\pi$-polarization). In Fig. 3(a), we also show as points the previous results on thermal lens in Yb:CALGO (see [15] and Refs. therein). The red square corresponds to $\boldsymbol{E} \perp \boldsymbol{c}$, while the two blue circles correspond to $\boldsymbol{E} \parallel \boldsymbol{c}$ taking into account the astigmatism of the thermal lens *id est* taking into account different radii of curvatures along the lens $\parallel \boldsymbol{a}$ or $\parallel \boldsymbol{c}$. The pump beam waist is $w_p = 200$ μm. The literature data agrees well with our calculations.

Figure 3(a) can explain the thermal mode stabilization and related polarization-switching observed previously for ***a***-cut Yb:CALGO crystal [15]. Let's consider a laser cavity having a stability limit due to positive thermal lens. At low pump power, $\sigma$-polarization will be naturally-selected due to higher gain. Then, at some pump level, optical power of thermal lens for this polarization will reach the stability limit, so cavity will not support oscillations at σ-polarization. As the gain cross-sections for both $\sigma$- and $\pi$-polarizations are very close [2] and ***a***-cut crystal provides access to both of them, the switch to $\pi$-polarization can occur. Indeed, laser cavity will be still stable again, as thermal lens will be weaker and stability limit will not be reached.

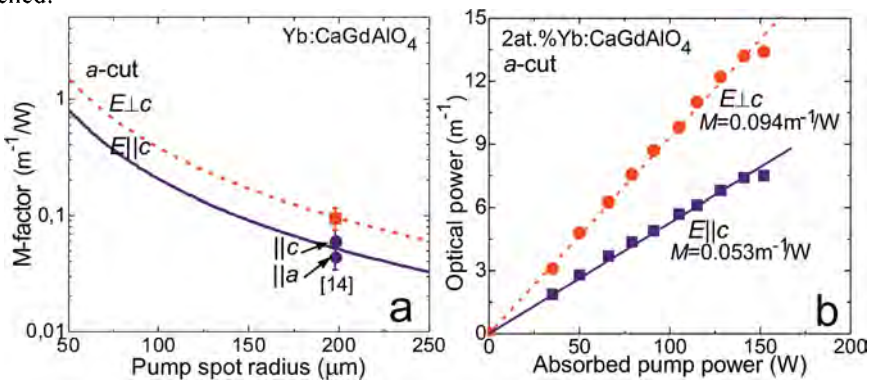


Fig. 3. (a) Sensitivity factor of thermal lens $M$ *vs.* pump spot radius $w_p$ for an ***a***-cut Yb:$CaGdAlO_4$ crystal: *points* are the experimental data from [15], *curves* are the calculation based on measured material parameters; (b) Optical power of thermal lens vs. absorbed pump power for an ***a***-cut 2at.%-doped Yb:$CaGdAlO_4$ crystal: *points* are the experimental data, *lines* are their fitting for calculation of $M$-factors.

In Table 3, we list the so-called "generalized" thermo-optic coefficient $\chi$ that determines overall variation of the optical path length in real laser element. For the three first columns, it has been determined using a 5at.%-Yb:CALGO. On the other hand, it was estimated in [15] from thermal lens measurements using a 2at.%-doped crystal. The difference between the TCOP and $\chi$ values allows for estimation of the impact of photoelastic effect. One can see that it is much stronger for $\pi$-polarization (as compared with $\sigma$ one). This explains higher distortions in the spatial profile of the laser beam after the "magic" mode switching.

In order to complete the thermo-optic characterization of Yb:CALGO, we perform direct measurements of optical power of thermal lens is an ***a***-cut crystal for both $\pi$ and $\sigma$ polarizations under high-power diode pumping. For this, a wavefront sensor based on lateral shearing interferometry was used. The probe beam was linearly polarized; the probe wavelength was 1.03 μm. For technical reasons, the studied crystal is a 2at.%Yb:CALGO, and has the dimensions of $2(\boldsymbol{c})\times 2\times 10(\boldsymbol{a})$ $mm^3$. It was placed into the V-shaped laser cavity and longitudinally-pumped from one side by a fiber-coupled laser diode at 980 nm. The crystal was mounted in copper holder that was water-cooled down to 18 °C. The average pump spot size in the crystal $w_p$ was 200 μm. All the measurements were performed in the lasing mode.

The results are shown in Fig. 3(b). As expected, the optical power of thermal lens depends linearly on the pump power. The slope of this dependency (sensitivity factor), $M = 0.094$ $m^{-1}$/W and 0.053 $m^{-1}$/W for $\sigma$ and $\pi$-polarizations, accordingly. This is in good agreement with our calculations, Fig. 3(a), $M = 0.095$ and $0.051 \pm 0.003$ $m^{-1}$/W.

Obtained sensitivity factors of thermal lens for an ***a***-cut Yb:CALGO crystal confirms the idea about its "athermal" behavior. Indeed, the $M$-values are near 5 times lower than that of $N_g$-cut Yb:KGW ($M \sim 0.5$ m$^{-1}$/W for the same $w_p = 200$ μm, recalculated from [26]). This crystal, another well-known material for short pulse generation, was considered previously to behave "athermally".

**5. Thermal conductivity**

In the present paper, CALGO crystals with low Yb doping ratio were studied (5at.% for d$n$/d$T$ measurements and 2at.% for thermal lens one). However, the important question is how to apply these results to highly-doped crystals (usable, for instance, in thin-disk lasers). It was shown that thermo-optic properties have a negligible difference versus the doping level, depending mainly on host [21], which is also experimentally confirmed for Yb:CALGO using the parameters obtained with the 2at.% and 5at.%-doped crystal, Fig. 3(a). In contrast, variation of thermal conductivity can be more profound. Thus, we aim to perform such a study for CALGO. It is well known that the thermal conductivity decreases versus the doping ratio. Indeed, the replacement of atoms of the lattice by the dopant creates disorder and perturbs the phonon propagation and thus reduces the thermal conductivity.

A following simple formula gives the evolution of the thermal conductivity $\kappa$:

$$\kappa = \frac{1}{\pi a_0}\sqrt{\frac{2k_B\nu\kappa_0}{\delta}}\,A\tan\left(\pi a_0\sqrt{\frac{\kappa_0\delta}{2k_B\nu}}\right), \tag{4}$$

taking into account the mass differences between the dopant ($M$) and substituted atoms ($M_i$) and the concentration substitution ($c_i$) given by the parameter ($\delta$):

$$\delta = \sum_i c_i\left(\frac{M_i - M}{M}\right)^2. \tag{5}$$

The other parameters are given elsewhere [27]. According to this formula, the substitution of $Gd^{3+}$ by $Yb^{3+}$ gives almost no change in the thermal conductivity (curve Gd100 in Fig. 5). Measurements are performed using a thermal conductivity analyzer from C-Therm technology TCi$^{TM}$. The experiment clearly indicates a much larger influence of the doping concentration on the conductivity. A hypothesis to understand this divergence is a partial substitution of Ca ions by Yb. Indeed, the Gd and the Ca share the same crystallographic $C_{4v}$-symetric site in CALGO, which favors this shared substitution. Various substitution ratios have been computed (Fig. 4) with different ratio of substitution from 100%-Gd/0%-Ca to 50%-Gd/50%-Ca. It appears that the best fit roughly corresponds to a partial repartition of the Yb-dopant on 80%-Gd/20%-Ca.

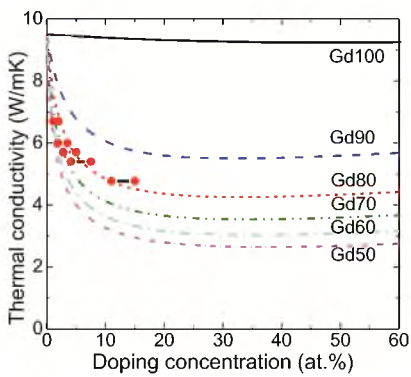


Fig. 4. Thermal conductivity versus doping concentration of Yb for Yb:$CaGdAlO_4$ crystal. Different curves represent the theoretical evolution considering various partial substitution of Gd and Ca by Yb: Gd100 means that Yb only substitute Gd, GdX means that Yb is replacing X% of Gd ions and 1-X% of Ca ions. The points are the experimental results. The line represents the difference between the nominal doping rate (higher number) to the actual one (lower number) measured by chemical analysis of the crystal.

One may notice in Fig. 4 that the experimental points do not follow exactly the 80%-Gd/20%-Ca curve. Indeed it appears that below 5% of doping the points are closer to the 70%-Gd/30%-Ca, which seems to indicate a variation of the ratio between the substituted ions with doping.

The anisotropy is also observed in the thermal conductivity. Indeed, the thermal conductivity along the ***a***-axis is better that the along the ***c***-axis. Nevertheless, the variation is only ±4.5 % compared to the average value and the impact on the thermal distribution anisotropy is then negligible. This is shown in Fig. 5 where the temperature mapping is given for an ***a***-cut 2(***c***)×2×10(***a***)-mm$^3$ crystal and a ***c***-cut 2(***a***)×2×10(***c***)-mm$^3$ crystal for comparison. The main differences observed comparing the different crystal orientations and pump-polarizations are clearly related to the variation of the absorption cross sections. To evaluate the difference of heat-removal efficiency between the ***a***-cut and the ***c***-cut, one can compare the thermal maps for an ***a***-polarized pump (which leads to the same thermal loading). In this case the temperature difference is only 4.5 % with a slightly anisotropic shape.

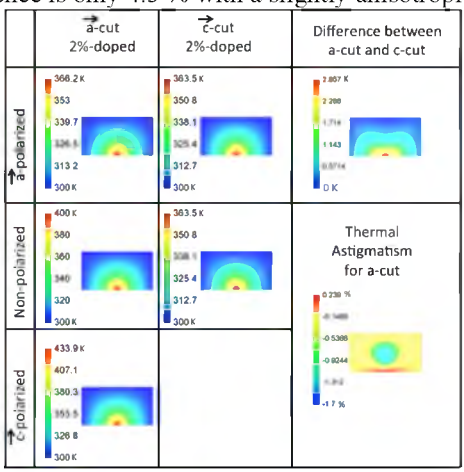


Fig. 5. Temperature elevation for 2%-Yb:CALGO with different orientations and pumping polarizations. The last column illustrates the thermal anisotropy.

To evaluate the anisotropy itself we also compare the thermal distribution of an ***a***-cut crystal with an equivalent isotropic crystal. One can clearly observe (Fig. 5, "thermal astigmatism for ***a***-cut") that the influence of the thermal anisotropy is far less important compared to the thermo-optic coefficient anisotropy impact. Indeed the impact of the thermal conductivity anisotropy in terms of temperature variation is only 2%.

## 6. Conclusions

In conclusion, we present complete experimental thermo-optic characterization of Yb:CALGO crystal, that includes measurements of d$n$/d$T$ and thermal coefficient of the optical path (TCOP) values, optical power of the thermal lens, thermal expansion and thermal conductivity coefficients. It is shown that large and negative d$n$/d$T$ values, as well as their anisotropy, are crucial for understanding of thermal-lens-driven effects in this material, like "athermal" behavior and unique mode stabilization by polarization-switching. The thermal conductivity evolution versus the doping has also been studied. And we demonstrate the low impact of thermal-conductivity anisotropy on the heat removal indicating the dominance of thermal expansion and thermal conductivity coefficients on the anisotropic thermal lens observed in Yb:CALGO.


## Acknowledgments

This work has been partially supported by the French National Research Agency (ANR) through the Femtocryble and Pampero programs and by the network CMDO+ from the CNRS.